SMART AND IOT BASED INTELLIGENT MONITORING OF DFIG GENERATOR SYSTEM FOR WECS

Abstract

The use and growth of renewable energy experienced a significant evolution in the past few decades. One of these energy sources that has a significant potential is wind power, which has become the focus of numerous studies. The dynamic simulation and management of a doubly fed induction generator (DFIG) using wind turbine (WT) systems are presented in this work. Because of their simplicity, proportional-integral (PI) based power controllers are frequently employed, however they have tuning issues. The indirect vector controlled VSI fed DFIG uses the Cascaded Adaptive Neuro-fuzzy based speed (ANFIS) controller presented in this paper to reduce torque ripple. When compared to standard PI controllers, the proposed cascaded ANFIS controller greatly minimizes torque ripple without the use of a filter and shows an efficiency of 97.62%. This paper's main contribution is IoT-based applications for wind energy conversion systems (WECS). Furthermore, simulations are given in the Matlab/Simulink framework to guarantee the controllers' approach.

Keywords: DFIG, WECS, PWM Rectifier, Cascaded ANFIS, IoT.

Authors

Viswaprakash Babu
Associate Professor
Pallavi Engineering College
Nagole, Hyderabad, India.
viswaprakash125@yahoo.com

K. Praveena
Assistant Professor
Department of Electrical and Electronics Engineering
Avanthi Institute of Engineering and Technology, Tagarapuvalasa
Andhra Pradesh, India.
veenaphilip2006@gmail.com

E. Maheswari
Associate Professor
Department of Electrical and Electronics Engineering
Sri Sai Ram Institute of Technology
Chennai, India.
maheswari.eee@sairamit.edu.in

A. R. Gayathri
Associate Professor
Department of Electrical and Electronics Engineering
Stella Mary's College of Engineering
Aruthengavillai, Nagercoil
ar.gayu13@gmail.com

I. INTRODUCTION

The development of renewable energy sources (RES) as an innovative approach to supplying the requirements of our community's energy needs. The generation of power using hydropower, solar, wind, geothermal, tide, wave, and biomass energy sources has received a lot of attention recently. The crucial factor in the expansion of wind power is thought to be energy [1]. To fulfill increasing energy needs, traditional exhaustion of resources increasingly prioritizes environmental protection and makes use of renewable energy sources. In comparison to the usual technique, the cost of producing energy is quite low. Future sustainable energy sources like wind energy are taken into consideration. Due to its many advantages over alternatives, DFIG is frequently utilized for the generation of electricity from wind energy [2, 3].

In comparison to wind turbines that employ fixed speed generators, the DFIG wind turbines flexibility in operating at various speeds based on the quantity of active and reactive power available makes the converter less expensive and reduces power losses. The enhanced capacity of the new specifications' variable speed WT to capture more wind energy and to provide greater power quality makes them profitable [4, 5]. Furthermore, by adjusting the speed of the turbine's output power, variable speed wind turbines reduce load stress on different structural parts of the turbine, such as the tower and blades. As a result, despite their substantial initial costs, wind turbines have become more accessible due to improvements in energy performance, longevity, and effectiveness. The rotor current and stator flux are controlled utilizing state feedback linearization procedures with the goal to outperform the exit strategy. Electromagnetic torque and stator current are examples of non-linear features required by the DFIG's dynamical architecture. The use of DFIG is expanding for a variety of reasons, including lowering mechanical stress, minimizing noise, and flexible regulation with the induction device and the electrical grid, consecutively converters provide active and reactive power [6–9].

The IoT has advanced to an entirely novel stage as a result of the importance of creating smart devices, intelligent manufacturing, and informational communications. IoT-based services are being adopted by numerous sectors to improve throughput and for handling data and analysis. These IoT based solutions are currently moving toward wind energy, the most encouraging, eco-friendly, and secure RES. They do this by utilizing cloud computing and big data analysis. Efficiency, performance, operational costs, and profit are crucial in the context of a global energy market. All of these factors call for a system that can continually evaluate efficiency and sustain it over time. For the long-term growth of the renewable energy industry, IoT analysis is viewed as an important technology development in this area [10, 11].

Traditional PI controllers are programmed for a single operational point, and when the point of operation modifications, they do not function effectively. Fuzzy or neural network-based controls are used in place of traditional PI controllers to solve this issue. The issue with fuzzy logic is that the function of membership and regulations must be determined with specialized knowledge. Neutral networks have the disadvantage that the direction of weight updates is determined by the derivative transfer operation, but the size of the derivatives has no bearing on the weight updates. Reactive power response is raised in an effort to decrease the machine’s performance [12–15]. The machine’s performance is increased, and the

transient influence on the overall system is decreased, using the cascading ANFIS control method.

This study presents intelligent monitoring of the DFIG generator system for WECS using smart and IoT technology. In this study, a PWM Rectifier and a PI controller based on the Cascaded ANFIS Controller are employed to improve the energy flow of a grid-integrated DFIG network. The structure of this work is as follows: The proposed model is explained in Section 2. The proposed System's modelling is created in Section 3. Section 4 displays the simulation findings. Section 5 of the paper's final conclusion provides details.

II. RELATED WORK

1. **Md Liton Hossain et al [2021]** [16] have made a study to pinpoint the power converter defect location in real time, this research suggests an innovative algorithm that will be included into the PI-SVPWM controller. To create WECS condition tracking across the IoT is needed for ensuring system resilience because the majority of wind power plants are either offshore or in remote places. In this research, a hardware prototype and industrial IoT algorithm are proposed for tracking WECS state in real-time environment. So that any possible harm to the WECS is avoided, a quick and suitable asset managerial choice may be made by authorised outsiders by tracking the status.

2. **Srikanth Velpula et al [2020]** [17] have suggested a quick and efficient method utilizing an admittance framework to assess the stability of SSTI. The suggested method provides a conductance-based sub synchronous parameter to determine the reliability of torsional couplings. The effect of the DFIG-WECS on the vibratory torsions of the neighbouring turbine generator is assessed using the sub synchronous conductance based technique. By the use of an admittance approach, the damping of the IGE and SSTI is examined at various wind speeds and compensation levels. Eigenvalue research and transient modelling are used to verify the admittance analysis findings. The results show that the damping of torsional modes is reduced by DFIG-WECS in the low frequency region of the sub synchronous network mode.

3. **Sambasivaiah Puchalapalli et al [2020]** [18] have explained a WECS that works with the grid and using a DFIG exchanges reactive power between two converters. If the wind speed is less than the rated wind speed, the rotor side converter (RSC) management of the DFIG is implemented to distribute reactive power, thereby reducing copper loss in the rotor winding. However, the RSC regulation has been developed to draw out the rated power without exceeding its rating and to maintain the stator terminal power factor at unity at the rated wind speed..

4. **Mohammad. I. Mosaad et al [2019]** [19] have proposed a novel DFIG- based WECS may operate more efficiently under wind surge and failure events if higher-temperature superconductors are incorporated into the DC connections of the rotor sides and grid side converters, which link the DFIG rotors to grid. The FOPI regulator is used to govern the transfer of energy among the SC and the system by regulating the frequency of operation of the DC chopper which links the SC with the DC link. SC's primary drawbacks are its cost and responsiveness to the controller that drives it.

2. **Abdelhak Djoudi et al [2018]** [20] have studied a DFIG-based WECS performs under erratic grid settings in terms of enhanced fault-ride-through and control. It introduces a sensor less rotor current, adaptive sliding-mode stator power regulation, and consistent frequency of switching. The suggested management approach is obtained directly from a nonlinear DFIG state approach, and the regulation rule is computed utilising the initial stator flux. It is important to note that the rotor current and flux are not sensed using any sensors in this control strategy. Furthermore, it is not necessary to extract the sequence components of the voltage, current, and flux data.

III. PROPOSED SYSTEM

The components of the wind generation system include a WT, a DFIG, a PWM rectifier, a controller, and a 1Ø voltage source inverter as depicted in Figure 1. For a grid-connected wind energy production system, a straightforward Cascaded ANFIS control technique is developed in this study.

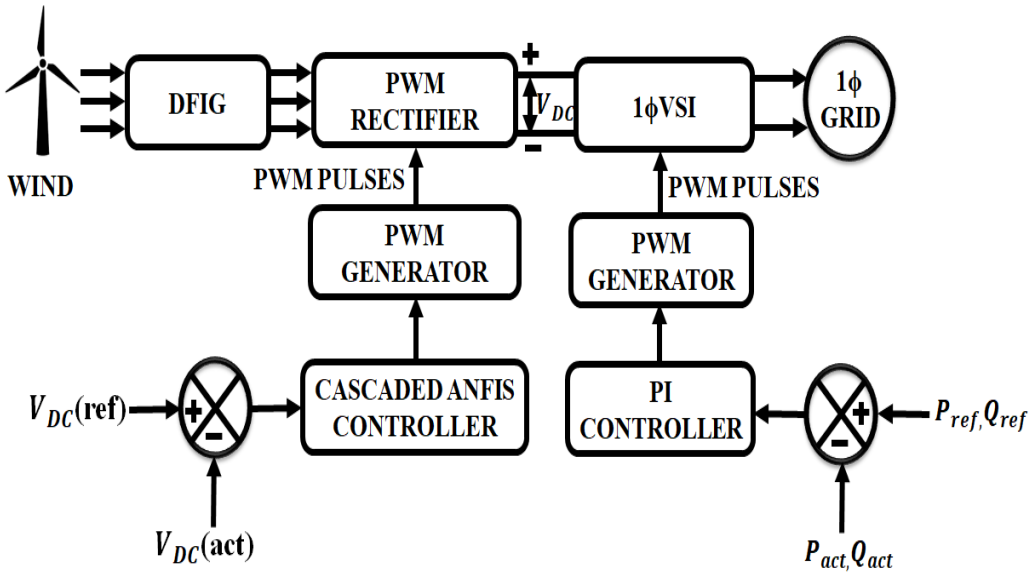

Figure 1: Proposed System Model

In this project, DFIG are powered by wind energy, which allows them to operate at rates that are approximately equal to or greater than their natural synchronous speed. The magnetic field is capable of being made to rotate by applying variable frequency AC power to the field windings, which enables adjustment of the motor or generator speed. For example, wind turbine generators can benefit from this. AC output voltage generated by the DFIG based WECS is unstable because of the wind's erratic behaviour. The DFIG-based WECS and PWM rectifier interface effectively remove fluctuations and convert AC voltage to DC voltage. PWM rectifier, which employs forced commutated power electronic semiconductor switches, is utilized for converting the AC power produced by DFIG to DC power, which is then sent to the grid via an inverter. When the input voltage to the inverter changes, cascaded ANFIS Controllers assist in keeping the output voltage constant. Cascaded ANFIS controller helps to eliminate harmonics from the produced reference current.

1. **Wind Turbine Model:** WT is a device that converts kinetic wind energy to electrical energy. WTs are developing into an increasingly important source of erratic renewable energy as a way to reduce energy costs and reliance on fossil fuels. Smaller wind turbines are used for things like battery charging and remote equipment like traffic warning signals. Larger turbines increase the amount of energy available to a home, and they can also use the electrical grid to return any excess energy to the utility company. There is an extensive selection of sizes for wind turbines, and they can have either horizontal or vertical axes though horizontal axes are more common.

   Following is a breakdown of the mechanical power a wind turbine can produce.

$$P_m = 0.5\rho A V_\omega^3 C_p(\lambda, \beta) \quad (1)$$

   When p is the air density, Rt is the WT's radius, and C_p is the power coefficient of the wind turbine, we get

$$C_p(\lambda, \beta) = 22\left(\frac{1.16}{\lambda_i} - 0.004\beta - 0.05\right)e^{-12.5\frac{1}{\lambda_i}} \quad (2)$$

$$\frac{1}{\lambda_i} = \frac{1}{\lambda + 0.08\beta} - \frac{0.035}{\beta^3 + 1} \quad (3)$$

   where, as shown below, λ stands for the tip speed ratio and β for the blade pitch angle.

$$\lambda = \frac{\omega_r R_T}{V_\omega} \quad (4)$$

   The dynamic model WT rotational speed ω_r is connected with the rotor speed ω_r as follows because a gearbox with the gear ratio n_g is present,

$$\omega_r = n_g \omega_r^{optimum} \quad (5)$$

   The torque equation for the generator's accurate dynamic model is provided by,

$$T_m \omega_r = P_m \quad (6)$$

   where T_m stands for rotor torque and ω_r for wind turbine speed; this ratio of wind power turbines is measured. The WT's power coefficient depends on its speed. The theoretical limit of C_p is 0.59, whereas the actual range is 0.2–0.4.

$$\omega_r^{optimum} = \frac{1}{R_T}\lambda_{optimum}\, n_g V_\omega \quad (7)$$

   At that moment in the calculation of the generator's rotor torque, which is related to the wind energy's maximum extraction $P_m\ max$,

$$T_m^{optimum} = 0.5\,\rho\pi R_T^5 C_P^{optimum}\, \omega_r^{optimum}\, (\lambda_{optimum}^3)^{-1} \quad (8)$$

It is clear that the wind turbine functions at its ideal speed of rotation and with the DFIG's maximum torque.

2. **Dynamic Model of the DFIG**: The grid converter, which injects reactive electricity into the grid, and the rotor converter, which regulates the generator speed, are both included in the power converter of the wind turbine generator. Figure 2 displays the actual and reactive power grid side converter modules.

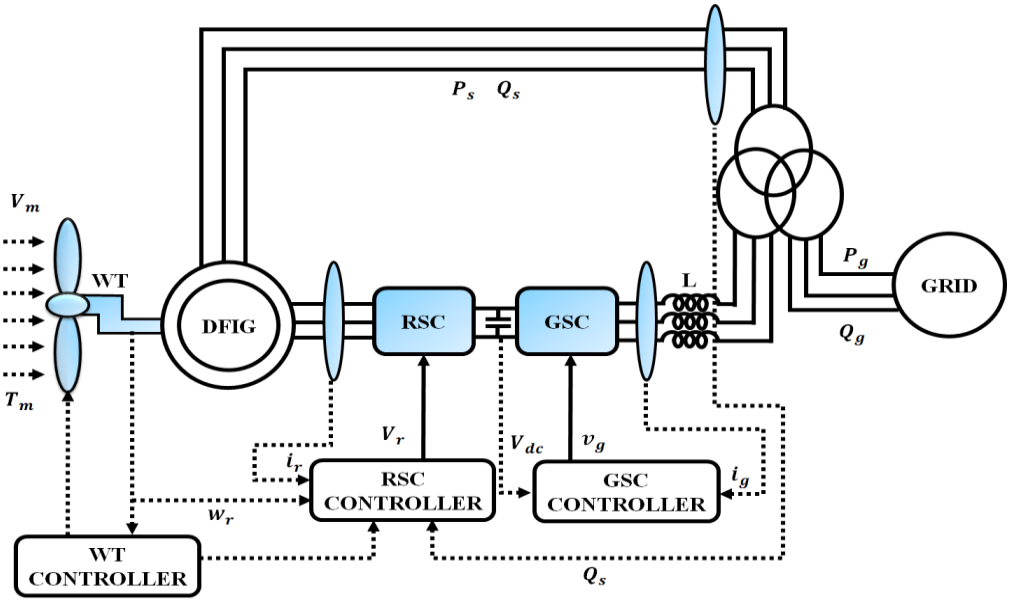

Figure 2: DFIG System

The following definitions apply to instantaneous power,

$$P_s = 1.5(V_{ds}I_{ds} + V_{qs}I_{qs}) \quad (9)$$

$$Q_s = 1.5(V_{qs}I_{ds} - V_{ds}I_{qs}) \quad (10)$$

$$P_g = 1.5(V_{ds}I_{dg} + V_{qs}I_{qg}) \quad (11)$$

$$Q_g = 1.5(V_{qs}I_{dg} + V_{ds}I_{qg}) \quad (12)$$

Where P_g and Q_g stand for the grid's active and reactive power, respectively, and P_s and Q_s stand for the DFIG's stator's active and reactive power, accordingly. The active and reactive powers typically define the DFIG wind turbine's nonlinear dynamic model. The stator voltage for DFIG is assumed to be roughly constant in order to reduce the dynamical framework. This supposition is utilized only when the system is in a stable state and the grid voltage variations at the PCC are typically less than 0.005 p.u.

3. **PWM Rectifier:** The conventional H-bridge rectifier features a straightforward circuit layout and a small number of components. Low cost and excellent efficiency are the results. Before choosing a particular energy storage part, the study that follows looks at a single phase PWM rectifier, as depicted in Figure 3. The subsequent calculations imply that the ac supply voltage us and current is sinusoidal

$$u_s(t) = U_s sin\omega t \quad (13)$$

$$i_s(t) = I_s \sin(\omega t - \varphi) \quad (14)$$

$$P_{in} = u_s(t) i_s(t) = \frac{U_s I_s}{2} \cos(2\omega t - \varphi) \quad (15)$$

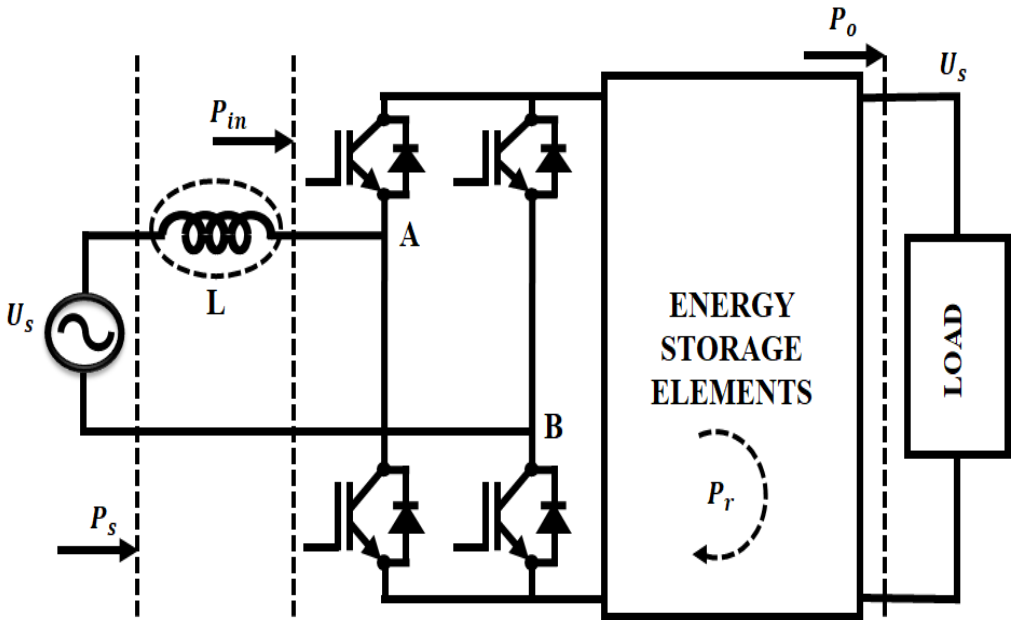

Figure 3: Single-Phase PWM Rectifier

The associated power is equal to the input inductor's energy, which may be represented as (16).

$$E_L = \frac{1}{2} L i_s^2 sin^2(\omega t - \varphi) \quad (16)$$

$$P_L = \omega L I_s^2 sin(\omega t - \varphi) cos(\omega t - \varphi) \quad (17)$$

L is the input inductance in this scenario. Subtracting (15) and (17) will give you the input power of the rectifier after the input inductor.

$$P_{in} = P_o + P_r = \frac{U_s I_s}{2} \cos(2\omega t - \varphi) + \frac{\omega L I_s^2}{2} sin(2\omega t - 2\varphi) \quad (18)$$

As we observe in (18), there are two components to the instant power: a constant power and a ripple power,

$$P_o = \frac{U_s I_s}{2} \cos\varphi \quad (19)$$

$$P_r = (\frac{U_s I_s}{2}\cos(2\omega t - \varphi) + \frac{\omega L I_s^2}{2} sin(2\omega t - 2\varphi)) \quad (20)$$

While the ripple power (21) is a second-order harmonic power that can be represented as follows, the constant power (22) supplies the dc load.

$$P_r = \sqrt{\frac{U_s^2 I_s^2}{4}} cos^2\varphi + (\frac{\omega L I_s^2}{2} - \frac{U_s I_s}{2} sin\varphi)^2 \times \sin(2\omega t - 2\varphi + \varphi) \quad (21)$$

$$I_s = \frac{2P_0}{U_s cos\varphi} \quad (22)$$

The ripple energy can be calculated as follows using the ripple power and peak current.

$$E_r = \frac{P_{r-peak}}{\omega} = \frac{\sqrt{P_0^2 + (\left(2\omega L {P_0^2}/{U_s^2 cos^2\varphi}\right) - P_0({sin\varphi}/{cos\varphi}))^2}}{\omega} \quad (23)$$

The dc load can only be protected against this ripple by using a substitute ripple energy storage system or component that must only function as a ripple filter.

4. **Cascaded ANFIS Controller:** A dimensionality curse and computing complexity are two drawbacks of the traditional ANFIS technique. The cascaded ANFIS technique, which is an extension of traditional ANFIS, overcomes these restrictions. The pair selection module and the training module, both important modules, are included. Figure 4 (a), depicts the cascaded ANFIS flow diagram.

Pair selection module- Figure 4 (b) provides an illustration of the pair selection module's overall process. The best matched pairing from the input variables is found in this case using an ANFIS architecture with two inputs and one output. The matched pair arrives as the result of the successive feature selection procedure used in this module. A nested loop is used to cycle through each combination of two pairs. The total amount of input variables is indicated by the word NI in Figure 4 (b). $Input_i$ and $Input_j$ have been selected as the system's inputs. The RMSE, denoted by the symbol E_P , is calculated and preserved for comparison with the RMSE's previous value (E_{prey}) . At the end of the second loop, the matching pair is determined by examining value with the lowest RMSE. Following the selection of the pairings, the training phase starts.

Train model module*:* The ANFIS model with two inputs, which are comparable to the pair selection component, is used by train model module. The matching pairs from pair selection module are given to it as input, and it produces outputs for each combination of inputs given. The operation ends when the target error is attained; if not, the subsequent iteration is carried out. Figure 5 displays the training module's functional flowchart.
Assume that the input variables for the optimization problems are X_1, X_2, X_3 *and* X_4

$$\text{Input} = \{X_1, X_2, X_3, X_4\} \quad (24)$$

The four input variables produce couples in the pair selection portion that match the best, as illustrated below:

$$\text{Input pairs} = \{X_1, X_3\}, \{X_2, X_1\}, \{X_3, X_4\}, \{X_4, X_1\} \quad (25)$$

ANFIS model with two inputs is utilized for each input pair to produce the following outputs:

$$RMSE = \sqrt{\overline{(A-P)^2}} \quad (26)$$

$$RMSE_{A,P} = [\sum_{i=1}^{N} \frac{(O_{Ai} - O_{Pi})^2}{N}]^2 \quad (27)$$

where N is the sample size and A and P are the actual results and expected results, correspondingly.

The selection of RMSE marks the conclusion of the initial iteration. Prior to moving on to the following iteration, the RMSE and goal error are contrasted.

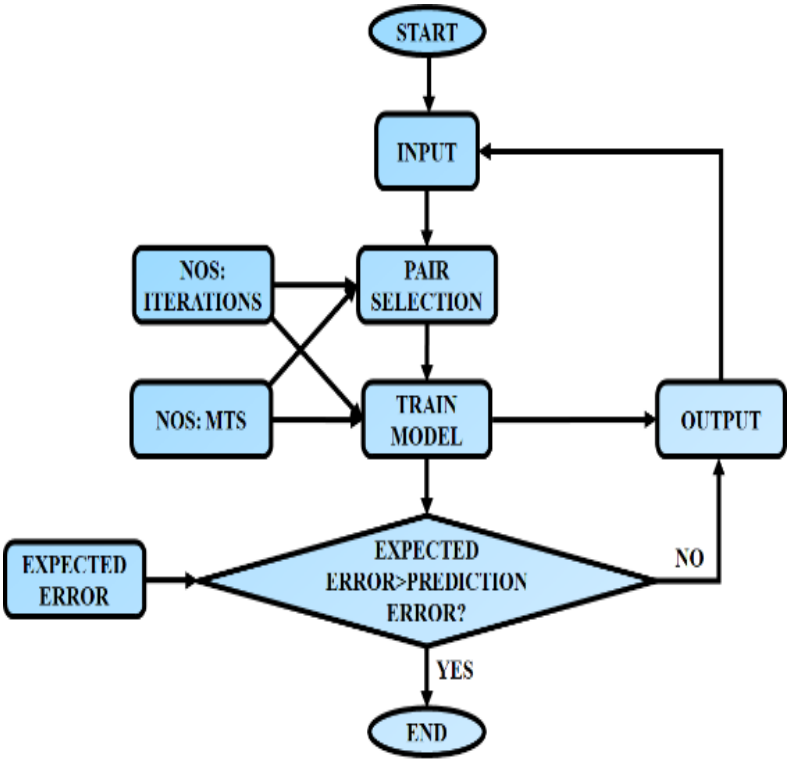

(a)

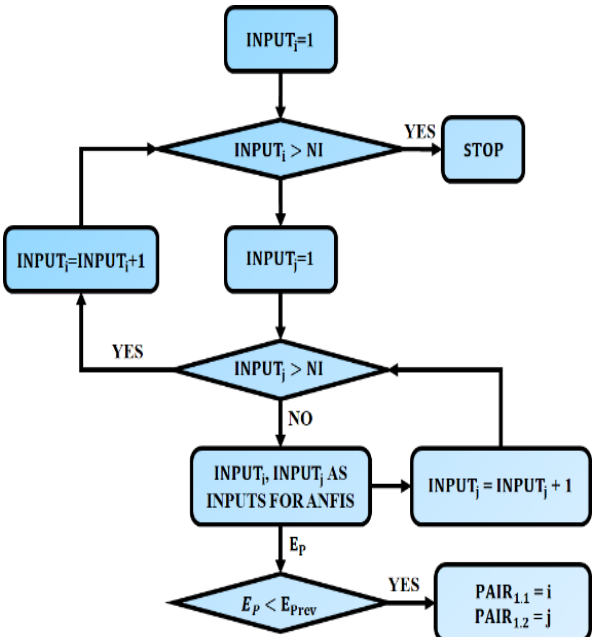

(b)

Figure 4: Flow Chart of Cascaded ANFIS (A) And Pair Selection Module (B)

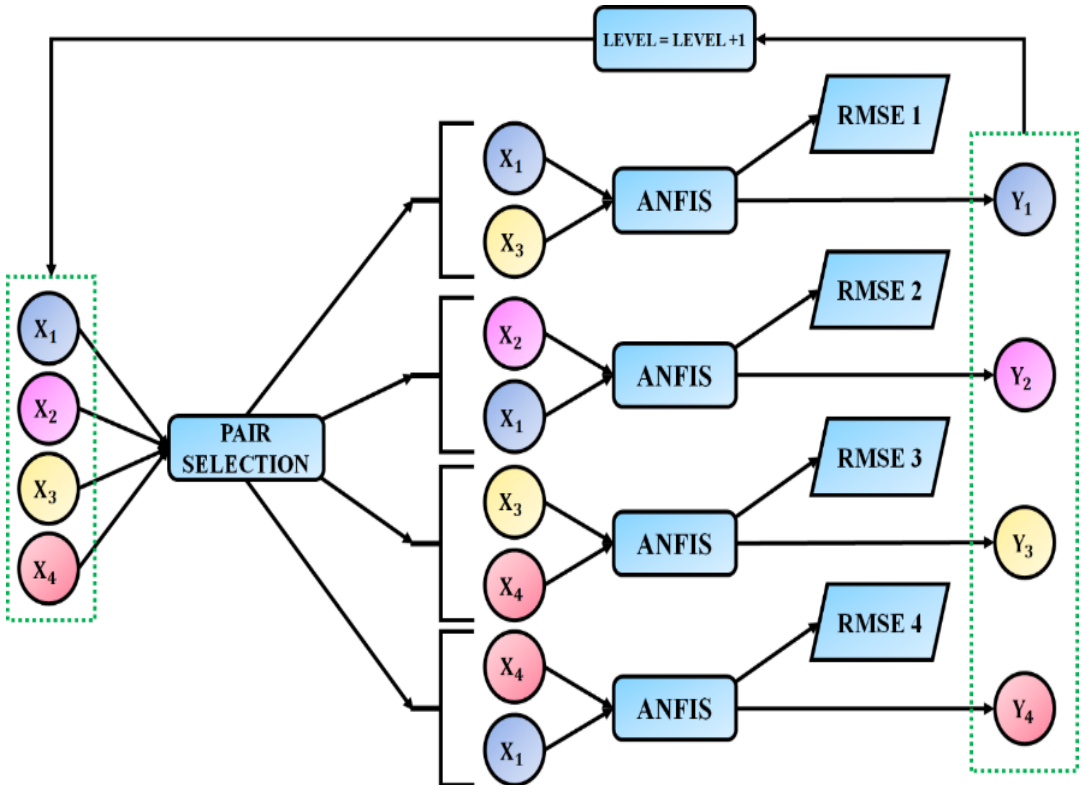

Figure 5: Structure of Training Module

5. **Grid-Connected VSI With LC Filter :** To manage the voltage of the filter capacitor, the inverter dynamic should have another voltage controller in front of the current controller. Fig. 16 depicts the per-phase equivalent circuit for the VSI linked to the grid with a filter. The analogous circuit allows us to write the system equations that change as

$$L_f \frac{di_{abc}(t)}{dt} = v_{abc}(t) - R_f i_{abc}(t) - u^c_{abc}(t) \quad (28)$$

$$C_f \frac{du^c_{abc}(t)}{dt} = i_{abc}(t) - i^j_{abc}(t) \quad (29)$$

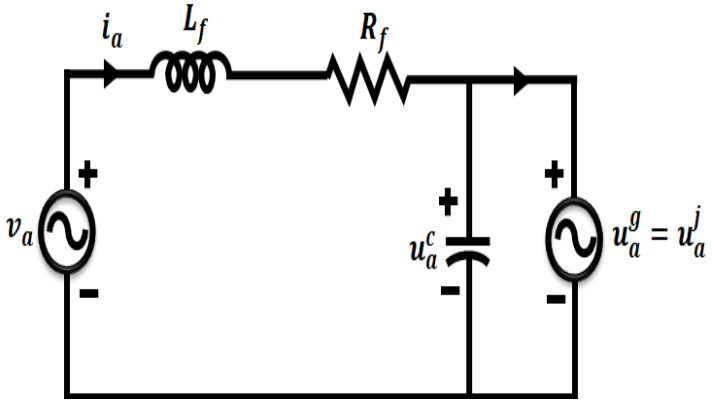

Figure 6: VSI with Filter Equivalent Circuit

The state equations can be used to explain the three phase modelling of the system when it is translated to a synchronous reference frame and axis is orientated with the grid voltage vector.

$$L_f \frac{d}{dt} i_d(t) = v_d(t) - R_f i_d(t) - u^c_d(t) + \omega_g L_f i_q(t) \quad (30)$$

$$L_f \frac{d}{dt} i_q(t) = v_q(t) - R_f i_q(t) - u^c_q(t) + \omega_g L_f i_d(t) \quad (31)$$

$$C_f \frac{d}{dt} u^c_d(t) = i_d(t) - i^j_d(t) + \omega_g C_f u^c_q(t) \quad (32)$$

$$C_f \frac{d}{dt} u^c_q(t) = i_q(t) - i^j_q(t) - \omega_g C_f u^c_d(t) \quad (33)$$

The isolation transformer between the grid and the inverter is going to be supplied to the main terminals of the system's inner control loop, which regulates the current flowing through filter inductor, and its outer control loop, which regulates the voltage of the filter capacitor. Because the injected current can be deemed a disturbance, the capacitor voltage may be adjusted by adjusting the filter inductor current. Consequently, the controller could be designed in a way that

$$i^r_d(t) = i^j_d(t) - \omega_g C_f u^c_q(t) + U^c_d \quad (34)$$

$$i^r_q(t) = i^j_q(t) - \omega_g C_f u^c_d(t) + U^c_q \quad (35)$$

If a controller is utilized, it might be programmed to do

$$U_d^c = k_p^c.\left[u_d^{c^r}(t) - u_d^c(t)\right] + k_i^c.\int\left[u_d^{c^r}(t) - u_d^c(t)\right]dt \quad (36)$$

$$U_q^c = k_p^c.\left[u_d^{c^r}(t) - u_q^c(t)\right] + k_i^c.\int\left[u_q^{c^r}(t) - u_q^c(t)\right]dt \quad (37)$$

Where the capacitor voltage controllers' proportional and integral gains, respectively, are denoted by k_p^c and k_i^c.

IV. RESULTS AND DISCUSSIONS

The proposed framework, adopts a novel PWM rectifier topology with Cascaded ANFIS controller to boost the wind generated for grid operation. The validation of proposed work utilizes MATLAB/Simulink software to develop a simulation model of the integrated wind grid-tied system with DFIG. Table 2 lists the design parameters of component involved in establishing the proposed system.

Table 1: Design Specification Parameters

Parameters	Ratings
Wind Turbine	
$No.of\ Turbines$	1
$Voltage$	$575V$
$Power$	$10\ kW$
$Battery$	48Ah, 48V

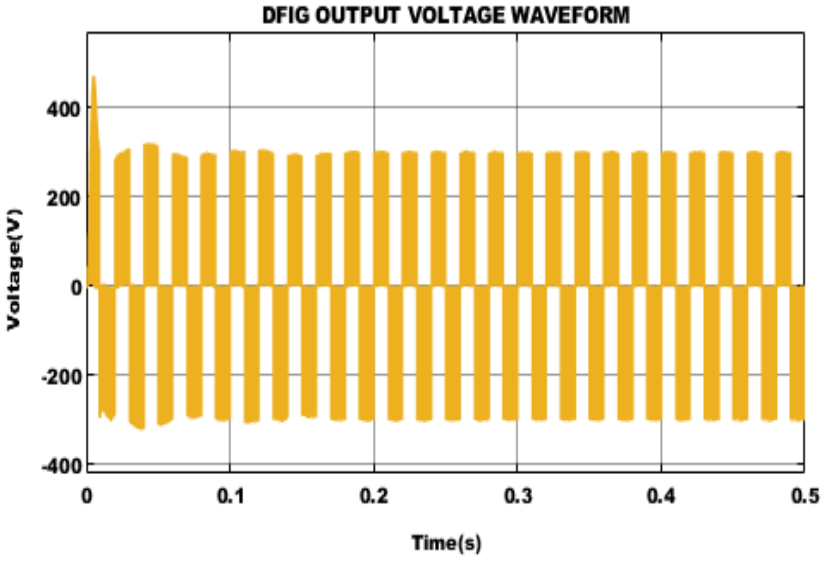

(a)

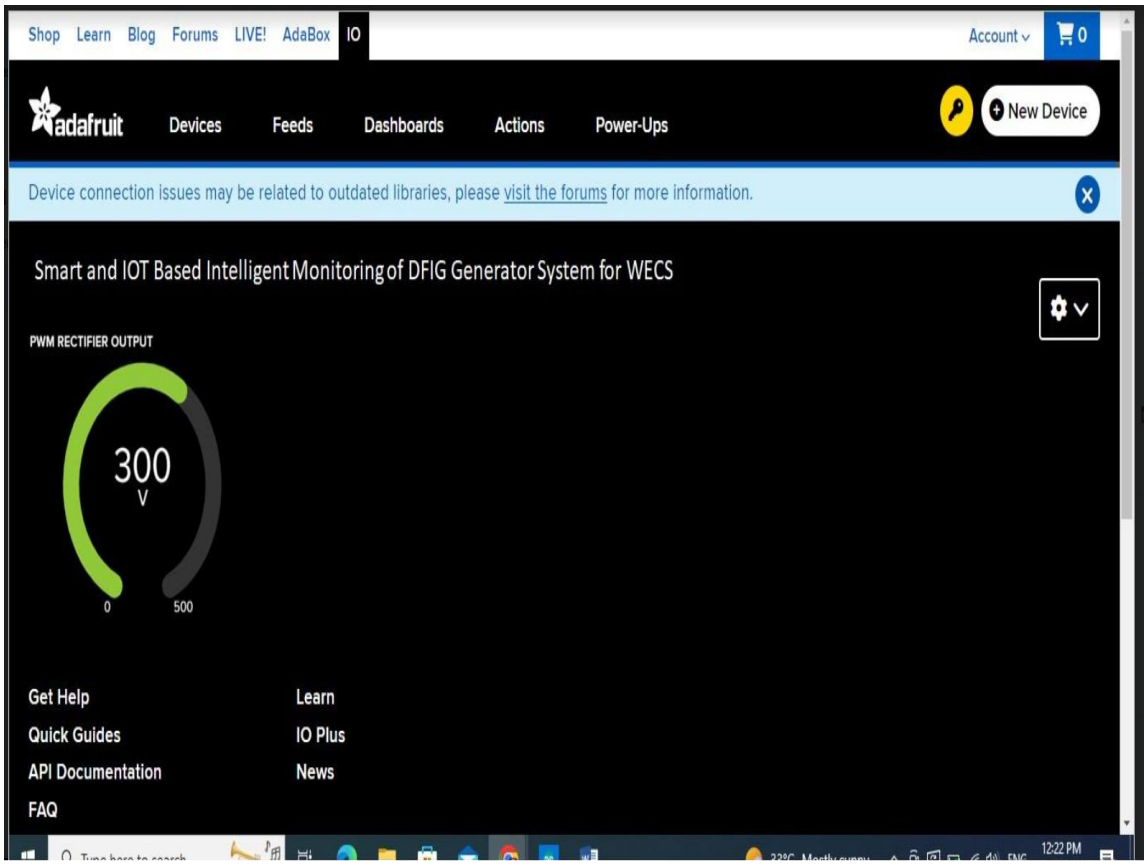

Figure 7: Output Voltage of the DFIG (a)MATLAB (b) IoT Blynk

Figure 7 shows the resulting waveform of the DFIG. The DFIG output briefly increases in voltage before remaining at 300V. The rectifier and PI controller are used to convert the received AC supply into DC. The output as a result demonstrates that after 0.01s, a steady DC value of 300V is maintained.

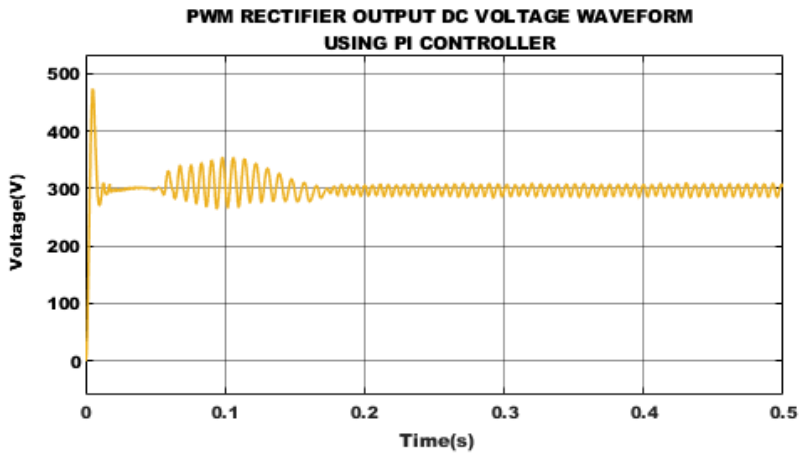

(a)

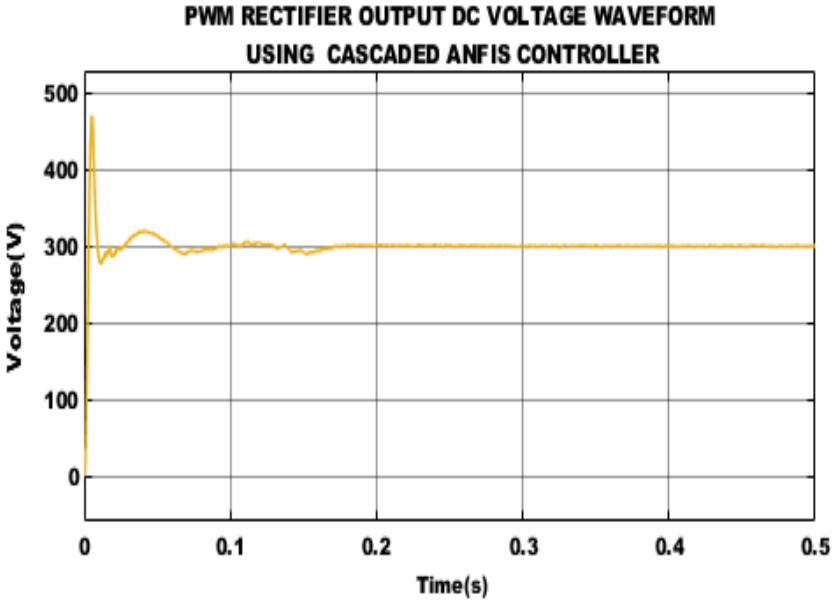

(b)

Figure 8: PWM Rectifier output using (a) PI controller (b) Cascaded ANFIS Controller

Figure 8 demonstrates how Cascaded ANFIS and PI controllers were used to control the DC link supply in order to achieve the PWM rectifier output voltage. Figure 7(a) makes it abundantly evident that tuning is necessary because a PI controller does not result in a stable voltage result of 300V. The Cascaded ANFIS controller generates output that is steady in Figure 7(b). In order to achieve stable DC voltage as soon as feasible and produce stabilized DC voltage of 300V, a cascaded ANFIS controller is recommended.

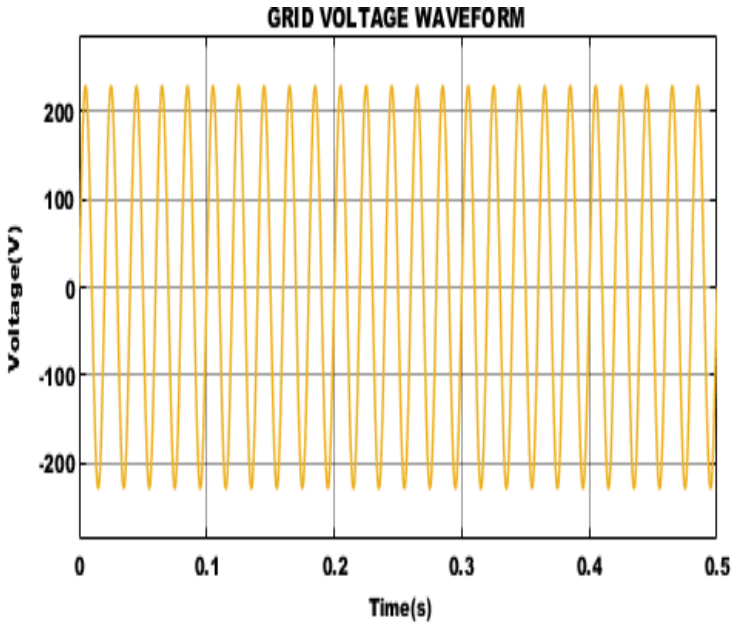

(a)

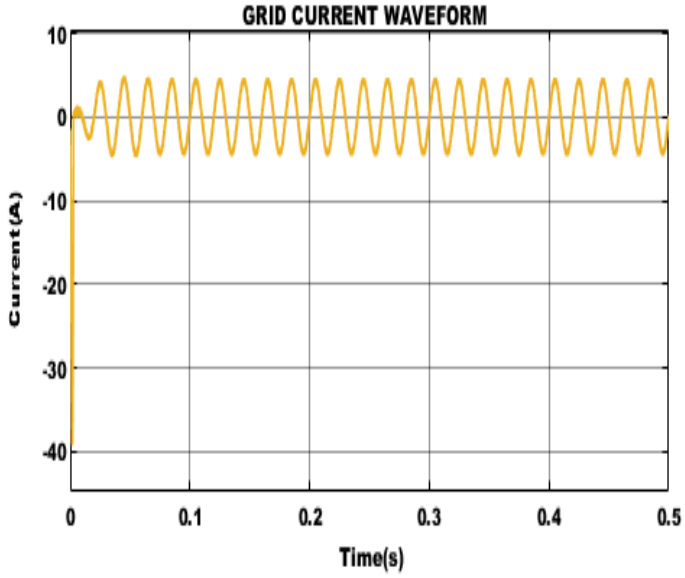

(b)

Figure 9: Grid waveform (a) Voltage (b) Current

The voltage and current waveform of a single-phase grid is seen in Figures 9(a) and (b), which symbolizes the various electrical energy patterns. Due to their regulated voltage and current, these waveforms offer a consistent and constant flow of electricity with effective energy transfer, effective operation of electrical devices, and maintenance of a steady system.

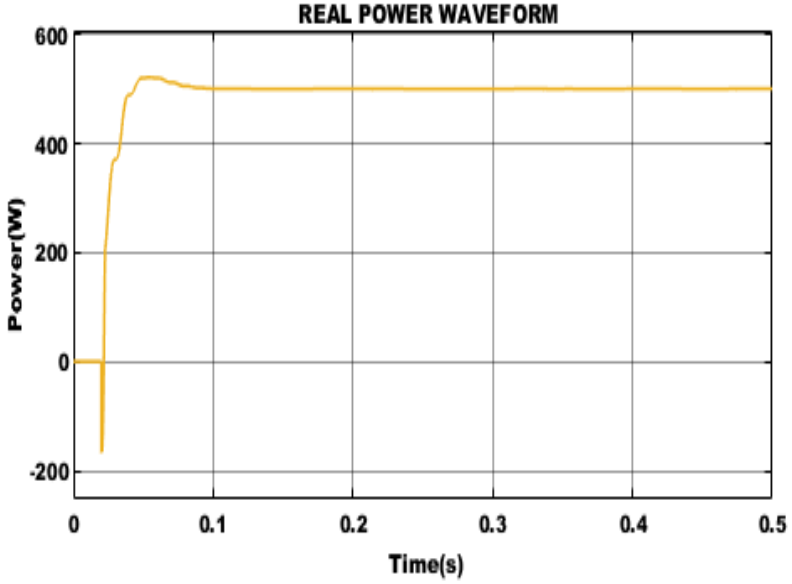

(a)

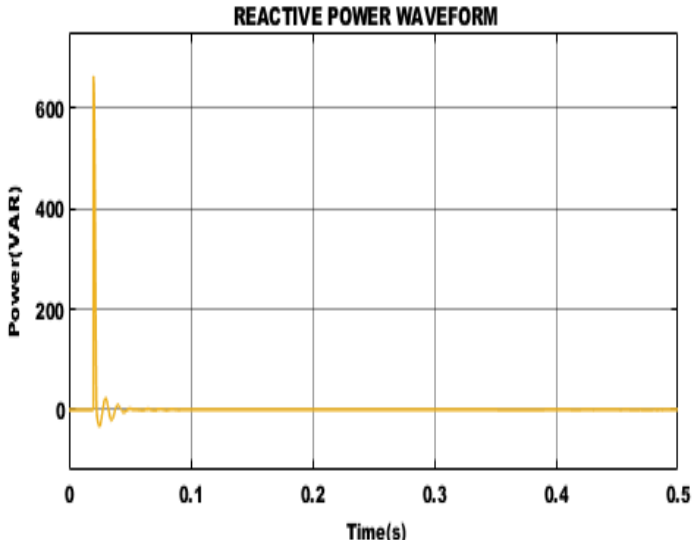

(b)

Figure 10: Power Waveform (a) Real (b)Reactive

Figure 10 displays the waveforms which demonstrate the grid's real and reactive power magnitude. Reactive power is significantly reduced in size compared to real power, which is 520 W.

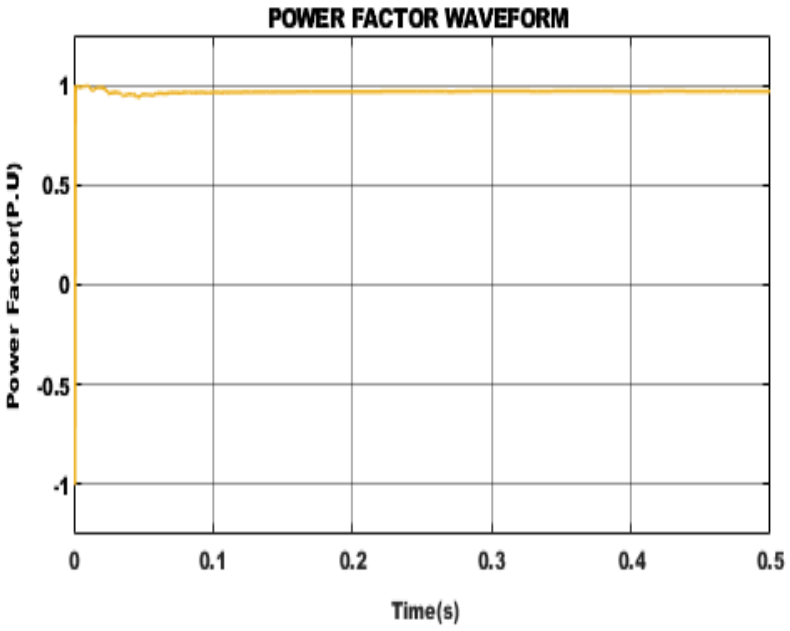

Figure 11: Power Factor Waveform

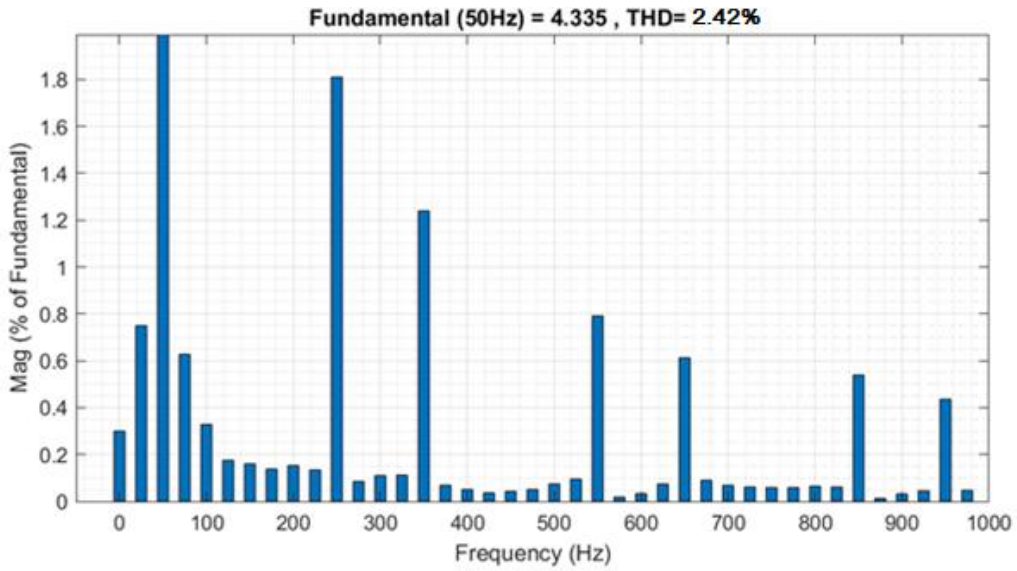

Figure 12: THD Value

The calculated percentage THD value of 2.42% is shown in Figure 12, validating the suggested methodology and its role in the THD minimization procedure. This decreased reactive power has a much smaller impact on voltage levels, preserving voltage stability and ensuring efficient grid synchronization.

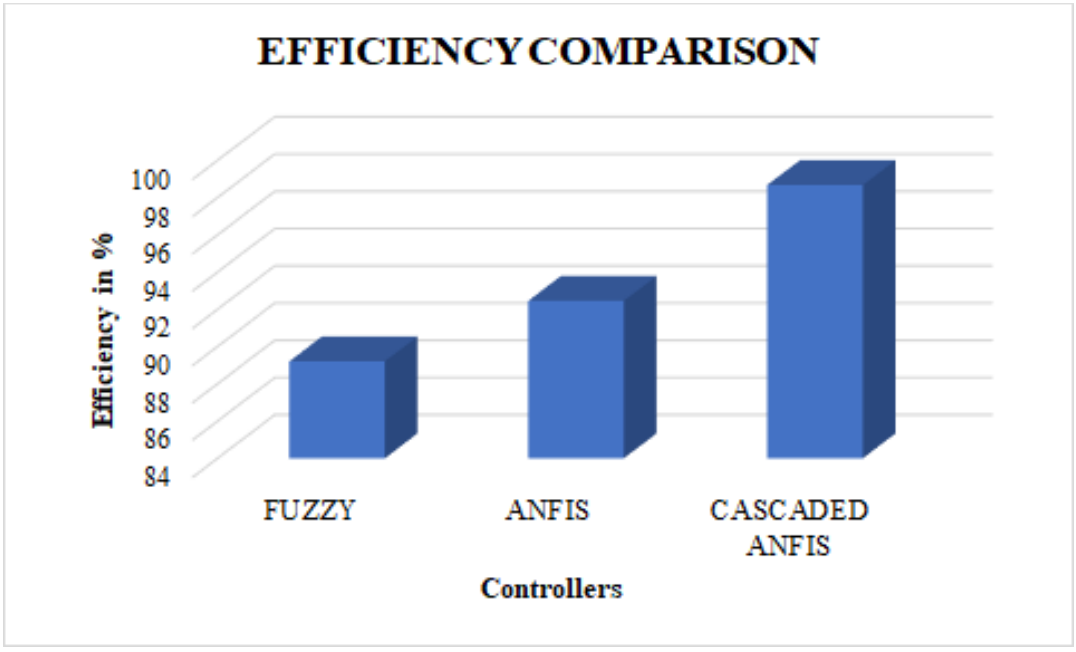

Figure 13: Comparison of Efficiency

Figure 13 depicts the efficiency comparison between the proposed Cascaded ANFIS controller design and traditional controllers. Analysis revealed that the suggested controller produced an increase in efficiency of 97.62%.

V. CONCLUSION

This study's goal is to increase the power drawn from wind energy while taking into account the fluctuating wind speed that interferes with energy production. Through recent developments and application of IoT in energy generation, particularly in connection to wind energy generation, we have managed the powers, whether they are active or reactive, given by the generator for this reason. This study looked at several IoT applications related to WT systems, including IoT integration with energy generation systems and IoT in systems for tracking, controlling, maintaining, and predicting wind turbines. A variable speed WT is coupled to a DFIG, and its modelling and control are investigated. The Cascaded ANFIS controller was used to simulate the efficiency of the PWM rectifier under various operating situations and shows an efficiency of 97.62%. The findings are then compared to those of the PI controller.

REFERENCES

[1] K. Amin and M. N. Uddin, "Nonlinear Control Operation of DFIG-Based WECS Incorporated With Machine Loss Reduction Scheme," in IEEE Transactions on Power Electronics, vol. 35, no. 7, pp. 7031-7044, July 2020.

[2] R. M. Prasad and M. A. Mulla, "Mathematical Modeling and Position-Sensorless Algorithm for Stator-Side Field-Oriented Control of Rotor-Tied DFIG in Rotor Flux Reference Frame," in IEEE Transactions on Energy Conversion, vol. 35, no. 2, pp. 631-639, June 2020.

[3] M. S. Yunus, A. Abu-Siada, M. A. S. Masoum, M. F. El-Naggar and J. X. Jin, "Enhancement of DFIG LVRT Capability During Extreme Short-Wind Gust Events Using SMES Technology," in IEEE Access, vol. 8, pp. 47264-47271, 2020.

[4] K. Wang, J. Zhang, Y. Pang, D. Xu and L. Pan, "Modeling of Nine-Switch-Converter Based on Virtual Leg and Its Application in DFIG Wind Generation System," in IEEE Transactions on Power Electronics, vol. 35, no. 7, pp. 7674-7688, July 2020.

[5] J. Samanes, E. Gubia, J. Lopez and R. Burgos, "Sub-Synchronous Resonance Damping Control Strategy for DFIG Wind Turbines," in IEEE Access, vol. 8, pp. 223359-223372, 2020.

[6] Y. Xia, Y. Chen, Y. Song and K. Strunz, "Multi-Scale Modeling and Simulation of DFIG-Based Wind Energy Conversion System," in IEEE Transactions on Energy Conversion, vol. 35, no. 1, pp. 560-572, March 2020, doi: 10.1109/TEC.2019.2953893.

[7] R. M. Prasad and M. A. Mulla, "A Novel Position-Sensorless Algorithm for Field-Oriented Control of DFIG With Reduced Current Sensors," in IEEE Transactions on Sustainable Energy, vol. 10, no. 3, pp. 1098-1108, July 2019.

[8] N. Jabbour, E. Tsioumas, C. Mademlis and E. Solomin, "A Highly Effective Fault-Ride-Through Strategy for a Wind Energy Conversion System With a Doubly Fed Induction Generator," in IEEE Transactions on Power Electronics, vol. 35, no. 8, pp. 8154-8164, Aug. 2020.

[9] N. Karakasis, E. Tsioumas, N. Jabbour, A. M. Bazzi and C. Mademlis, "Optimal Efficiency Control in a Wind System With Doubly Fed Induction Generator," in IEEE Transactions on Power Electronics, vol. 34, no. 1, pp. 356-368, Jan. 2019.

[10] Singla, Manish Kumar, Jyoti Gupta, Parag Nijhawan, Souvik Ganguli, and S. Suman Rajest. "Development of an Efficient, Cheap, and Flexible IoT-Based Wind Turbine Emulator." Business Intelligence for Enterprise Internet of Things, pp: 225-231, 2020.

[11] Musyafa, Ali, F. C. Aguisti, R. D. Noriyati, I. Abadi, H. Harsono, and Muhammad Khamim Asy'ari. "Design and Development of a Vibration Monitoring For Wind Turbine System Reliability Evaluation Based of Internet of Things (IoT)." International Journal of Mechanical & Mechatronics Engineering, Vol. 20, no. 5, pp: 96-105, 2020.

[12] R. Errouissi, A. Al-Durra and M. Debouza, "A Novel Design of PI Current Controller for PMSG-Based Wind Turbine Considering Transient Performance Specifications and Control Saturation," in IEEE Transactions on Industrial Electronics, vol. 65, no. 11, pp. 8624-8634, Nov. 2018.

[13] P. Mani, J. -H. Lee, K. -W. Kang and Y. H. Joo, "Digital Controller Design via LMIs for Direct-Driven Surface Mounted PMSG-Based Wind Energy Conversion System," in IEEE Transactions on Cybernetics, vol. 50, no. 7, pp. 3056-3067, July 2020.

[14] P. Mani, R. Rajan, L. Shanmugam and Y. H. Joo, "Adaptive Fractional Fuzzy Integral Sliding Mode Control for PMSM Model," in IEEE Transactions on Fuzzy Systems, vol. 27, no. 8, pp. 1674-1686, Aug. 2019.
[15] T. D. Do, "Disturbance Observer-Based Fuzzy SMC of WECSs Without Wind Speed Measurement," in IEEE Access, vol. 5, pp. 147-155, 2017.
[16] M. L. Hossain, A. Abu-Siada, S. M. Muyeen, M. M. Hasan and M. M. Rahman, "Industrial IoT based condition monitoring for wind energy conversion system," in CSEE Journal of Power and Energy Systems, vol. 7, no. 3, pp. 654-664, May 2021.
[17] S. Velpula, R. Thirumalaivasan and M. Janaki, "Stability Analysis on Torsional Interactions of Turbine-Generator Connected With DFIG-WECS Using Admittance Model," in IEEE Transactions on Power Systems, vol. 35, no. 6, pp. 4745-4755, Nov. 2020.
[18] S. Puchalapalli, B. Singh, S. K. Tiwari and P. K. Goel, "Design and Analysis of Grid-Interactive DFIG Based WECS for Regulated Power Flow," in IEEE Transactions on Industry Applications, vol. 56, no. 5, pp. 5396-5407, Sept.-Oct. 2020.
[19] Mohammad. I. Mosaad, A. Abu-Siada and M. F. El-Naggar, "Application of Superconductors to Improve the Performance of DFIG-Based WECS," in IEEE Access, vol. 7, pp. 103760-103769, 2019.
[20] Djoudi, S. Bacha, H. Chekireb, H. Iman-Eini and C. Boudinet, "Adaptive Sensorless SM-DPC of DFIG-Based WECS Under Disturbed Grid: Study and Experimental Results," in IEEE Transactions on Sustainable Energy, vol. 9, no. 2, pp. 570-581, April 2018.

